RSC Advances

ROYAL SOCIETY OF CHEMISTRY

www.rsc.org/advances

Submit to RSC Advances

Situ Polymerized PEDOT/Fe_3O_4 Composite as Pt-free Counter Electrode for high efficient Dye Sensitized Solar Cells

Min Zheng, Jinghao Huo , Yongguang Tu, Jinbiao Jia，Jihuai Wu*, Zhang Lan

Engineering Research Center of Environment-Friendly Functional Materials, Ministry of Education,

Institute of Materials Physical Chemistry, Huaqiao University, Quanzhou 362021, China

Abstract: 3,4-ethylenedioxy thiophene (EDOT) precursor solution doped by Fe_3O_4 was spin-casted onto fluorine doped tin oxide (FTO) glass and form poly(3,4-ethylenedioxy thiophene) (PEDOT)/Fe_3O_4 hybrid films by situ polyreaction. The films are utilized as counter electrode of dye Sensitized Solar Cells (DSSCs). Photoelectric conversion efficiency (PCE) for DSSCs based on PEDOT/Fe_3O_4 varied with the different content of Fe_3O_4 in precursor solution. When the content of Fe_3O_4 was 2mg/ml in precursor solution (PEDOT/ Fe_3O_4-2), reveals the best performance (8.69%). And, that of DSSC based Pt counter electrode is 8.35%. According surface micro topography and electrochemical analysis, large active areas ,consecutive electronic transmission channel and lower charge transfer resistance could be responsible for the high PCE.

Introduce：

Since M.Gratzel et.al made a breakthrough in 1991[1], dye sensitized solar cells (DSSCs) have attracted much attention due to their low cost, easy preparation, good performance and environmental benignity. The task of counter electrode is the reduction of the redox species used as catalyst and collecting electrons from external circuit. As we know, noble metal Pt reveals the optimal performance now and different kinds of CEs have been studied to replace Pt CEs, for example, Carbon materials[2-4], conductive polymer materials[5-8], transition metal sulfides and

* Corresponding author. Tel.: +86 595 22693899; fax: +86 595 22692229.

E-mail address: jhwu@hqu.edu.cn (J. Wu).

diseleniums[8-10], alloy metal[11, 12]. However, there remain some deficiencies to be overcome, such as complicated preparation, difficult large-area applications, unstability and so on. Hence, developing a CE which has low cost, a flexible procedure and high catalytic activity is significative[13, 14].

Poly (3, 4-ethylenedioxythiophene) (PEDOT) is one of the most widely investigated conducting polymer because of its attractive properties such as low band gap, remarkable environmental stability, high electrical conductivity and transparency[15, 16]. Moreover, Yohannes and Inganas[17] found this material has excellent catalytic activity for I^{3-}/I^- reduction and their study revealed the PEDOT could be as a CE potential material for DSSCs. However, many researchers showed that the pure PEDOT CE can not generated an satisfied cell efficiency compared with Pt-based DSSCs. So the modifications by incorporating with nanomaterials have been suggested. It was reported that PEDOT/carbon[18-20], PEDOT/metal[21, 22], PEDOT/metal oxide[23, 24], PEDOT/metal carbides or Metal nitride composites[25, 26] researched as the counter electrode. Among them, the PEDOT/metal oxide showed a prominent performance. Maiaugree et al.[23] and Hu[24] and his coworkers explored PEDOT/TiO_2 and PEDOT/ZnO as DSSCs counter electrodes and got photoelectric conversion efficiency (PCE) of 8.49% and 8.17%, respectively. While, little investigation has been conducted on PEDOT metal oxides as DSSC counter electrode catalysts. Fe_3O_4 has attracted attention because of its catalysis, high electronic conductivities, low cost and environmental benignity. Ma et al.[27] synthesized micron-sized Fe_3O_4 "flowers" and rosin carbon/Fe_3O_4 composite as the counter electrode and achieved 7.65% and 8.11% as values for PCE, respectively.

Herein, the composite film consisted PEDOT and Fe_3O_4 nanoparticles was prepared with a simple in-situ polymerization and applied to the counter electrode for DSSCs. The concentration of Fe_3O_4 can varied from 0mg/ (ml precursor solution) to 3mg/ (ml precursor solution) and the catalysis of the composite is different. The best PCE achieved 8.69% when the concentration of Fe_3O_4 was 2mg/(ml precursor solution),followed by DSSCs with Pt(8.38%).

Experiment

2.1 Preparation of Fe_3O_4 Nanoparticles

Fe_3O_4 was synthesized with a wet chemical method based on hydrolysis of Fe^{3+} and Fe^{2+} salts in the presence of NaOH as the previous study[28]: $FeCl_2 \cdot 4H_2O$ (1M) dissolved in the $NaOH \cdot FeCl_3$ (2M) aqueous solution. After stirring for 30min at room temperature, NaOH solution (2M) was added dropwise until the PH of the reaction mixture solution was adjusted to 11-12. Finally, black Fe_3O_4 precipitate was obtained and collected by a strong magnent. These particles were washed several times with distilled water and alcohol and dried at 80℃ in vacuum oven for 12h.

2.2 Fabricate the PEDOT/Fe_3O_4 counter electrode

Fe3O4 (0.1g/ml) was diffused in absolute ethyl alcohol by ultrasound equipment and mechanical agitation. EDOT (0.6g), Polyvinyl-pyrrolidone (PVP, 0.2g), pyridine(0.1ml) were dissolved in 10ml absolute ethyl alcohol, stirred for 10 mins. The solution was added dropwise into 10ml Iron (III) p-toluene-sulfonate (2g) ethanol solution with vigorously stirring. 0ml, 1ml, 2ml,3ml Fe3O4 suspension were added into 5ml the mixture solution respectively (corresponding to PEDOT,PEDOT/Fe3O4-1, PEDOT/Fe3O4-2 and PEDOT/Fe3O4-3) and all of the solutions were diluted to 10ml. Spin-coated 100ul diluted prepolymer onto the 1.7 ×1.7cm2 FTO glasses (sheet resistance 14Ω □-1, Nippon Glass Co. JP) on 500rpm for 2s by KW-4A spin processor, leaving a homogeneous prepolymer liquid films on the FTO glass, and let these films stand for 1 min . Then repeated three times and let them stand for half an hour in the air. Lastly, the films were washed with ethanol to colourless and dried at 80℃.

3.3. Preparation of TiO_2 photoanode and fabrication of DSSCs

The TiO_2 blocking layer and the mesoporous TiO_2 electrode preparation are described in the literature[29, 30]. A dye was loaded on the film by immersing the TiO_2 film in a 0.3 mM dye N719 ethanol solution for 18~24 h. A dye-sensitized solar cell (DSSC) was assembled by the methods as described previously[30].

2.4. Characterization

Powder X-ray diffraction (XRD) analysis was performed by a Bruker D8 Advance X-ray diffractometer using Cu Ka radiation (λ = 1.5418 Å), operating at 40 kV/20mA. The surface micro

topography were observed by a field emission scanning electron microscopy (FESEM, S-8000, HITACHI). The field emission scanning electron microscopy (FESEM) photos were carried out on a JME-2100 transmission electron microscope operating at an accelerating voltage of 200 kV. Fourier transform infrared spectroscopy (FTIR) analysis was observed on a monocrystalline silicon piece. All of electrochemical measurements were carried out with an electrochemical workstation (Zennium/IM6, Zahner, Germany). Photovoltaic parameters of DSSCs were recorded with KEITHLEY Model 2450 quick star guide under illumination by Newsport 91150V solar simulator (AM 1.5, 100 $mW \cdot cm^{-2}$).

3. Results

3.1. Compositions and morphology analysis

Fig.1 shows the surface morphologies of PEDOT and PEDOT/Fe_3O_4 composite. In fig.1 (a), a relatively flat and smooth surface with crarizonae was observed. Fig .1(b)-(d) suggests that the composite films have rougher surface morphology. As we can see, when the Fe_3O_4 content is 1mg/ml (fig .1(b)), the film is composed with 100-200nm lumps and some shot rodlike particles containing some tiny particles. Moreover, among these large particles, there are some Micropore-mesopore structure. With the increase of Fe_3O_4, the number of lump structures increases (fig.1 (c)). The particles in the film of PEDOT/Fe_3O_4-3 was smallest, and the large particles almost disappear. Meanwhile less porous can be observed (fig.1 (d)). Fig.1 (e) shows the section view SEM image of PEDOT/Fe_3O_4-2 and one can see that the thinkness of the film is about 200nm.

To clarify the element of the composite, FTIR experiments and XRD were carried out. Fig.1 (g) reveals the XRD pattern of the final Fe_3O_4, which is in good agreement with Fe_3O_4 (JCPDS #75-0449). In Fig.1(g) ,the 2θ diffraction peaks at 30.36°, 35.8°, 43.5°, 57.5° and 63.15°, which is assigned to the Fe_3O_4 planes of (220), (311), (400), (511), and (440), respectively.

Fig.1 (f) shows the FTIR spectroscopy of EDOT (A) and PEDOT (B). Characteristic peaks of EDOT are mainly observed at 1750cm^{-1}-500cm^{-1} in curve. Two strong and sharp absorption bands at 1522$cm^{-1}$and 1486 cm^{-1} arise from asymmetrical stretching vibration and symmetrical stretching vibration of C=C in the thiophene ring, respectively. The peaks at 1365cm^{-1}, 930cm^{-1} and 892cm^{-1} respectively originate from the C-C stretching modes, C-S stretching vibration and unsaturated hydrocarbon keys in the thiophene ring. From curve (B) intensity of

absorption characteristic bands from PEDOT decrease and the peak position shift. In the thiophene ring, the bands due to the asymmetrical stretching vibration of C=C, the stretching modes of C-C and the stretching vibration of C-S shift to near the wavenumbers of 1515cm^{-1},1332 cm^{-1} and 981 cm^{-1}, respectively. Meanwhile, the peak of unsaturated hydrocarbon keys disappear, suggesting that polymerization pattern of EDOT is α-α'.[15]

Here is Fig.1

3.2 Photovoltaic performance of DSSCs

Here is Fig.2

The performance for the DSSCs based on different counter electrodes was measured under one illumination (AM 1.5 G, 100mWcm^{-2})and PCE and fill factor are calculated according to the following equations[31]:

$$PCE=\frac{JmaxVmax}{Pin}\times 100\%=\frac{JscVocFF}{Pin}\times 100\% \quad (1)$$

$$FF=\frac{JmaxVmax}{IscVoc} \quad (2)$$

Where J_{SC} is short-circuit current density, J_{max} is current density at maximum power output, and V_{OC} is open-circuit voltage, V_{max} is the voltage at maximum power output. Here, P_{in} is the luminous flux which shined on the DSSCs.

In order to determine the optimal thickness of the counter, the films were prepared by spin coating

PEDOT/Fe_3O_4-2 precursor solution from one to four times and the J-V curves are shown in fig.2 (a) and the results are shown in Table 1. The thinner counter electrode film revealed a bad performance and as the thickness increased, the performance of counter electrode became better. However, when the number of spin-coating was over there times, the PCE of DSSC decreased. In our opinion, as precursor solution kept on the FTO was skimpy, the polymerization product (PEDOT) was also skimpy. AS a result, the film was imperfect and the catalytic properties was not satisfactory. But, too much precursor solution kept on the FTO brought a thick electrode film and the electronic transmission distance in the counter electrode became longer. In a word, spin-coating the precursor solution for there times and a about 200nm thick film (Fig.1(e)) was appropriate.

The J-V curves of DSSCs based on different counter electrodes are shown in Fig.2 (b) and photovoltaic parameters are listed in Table 2. It is seen that the V_{OC}, J_{SC}, FF, and PCE are 0,740V,

16.3 mA.cm^{-2}, 0.615 and 7.40 %, respectively, for DSSCs with situ-Polymerized PEDOT. When the pure Fe_3O_4 was used as CE, the DSSC showed a poor photovoltaic performance (PCE=4.02%). Interestingly, when Fe_3O_4 was added in CEs as additive, the photovoltaic performance varied obviously. V_{OC} of DSSCs based PEDOT/Fe_3O_4 changed slightly, but the value of J_{SC} and FF are dependent on the Fe_3O_4 content in the composite CEs. Both J_{SC} and FF went to the maximum value in the DSSCs with PEDOT/Fe_3O_4-2, as a result, the PCE of the DSSCS with PEDOT/ Fe_3O_4-2 is optimal (8.69%). Compared with Pt CEs (PCE=8.35%), PEDOT/ Fe_3O_4-2 also revealed good performance: an equal FF and a larger J_{SC} brought a slightly higher PCE value. Several reason could be under consideration including active area, catalytic activity and film conductivity for CEs. To analyze these character, Cyclic Voltammetry (CV), electrochemical impedance spectroscopy (EIS) and Tafel polarization measurements were conducted.

Here is Table 1

Here is Table 2

3.3 Electrochemical measurement

To examine the reduction reaction of I_3^- on the CEs, the cyclic voltammogram (CV) tests were carried out. The cyclic voltammograms (CVs) of samples was measured in a three-electrode electrochemical cell with an electrochemical workstation (CHI 660C, Shanghai Chenhua Co., Ltd, China) by using a CE as working electrode, a platinum wire electrode as counter electrode, a saturated Ag/AgCl electrode as reference electrode. Fig. 3(a) shows the CVs for PEDOT, PEDOT/Fe_3O_4, Pt and Fe_3O_4 electrodes at a scan rate of 50 mV·s^{-1}, and two pairs of redox peaks (OX_1 and RED_1, OX_2 and RED_2) can be observed in all of spectrograms, which demonstrates that all kinds electrodes can reduce I_3^- to I^- in order to ensure the dye's renewability.

The reduction reactions on cathodic electrode and the oxidation reactions on anode can be assigned as follows[32]:

OX_1 at anode: $3I^- \longrightarrow I_3^- + 2e^-$ (3)

OX_2 at anode: $2I_3^- \longrightarrow 3I_2 + 2e^-$ (4)

RED_1 at cathode: $I_3^- + 2e^- \longrightarrow 3I^-$ (5)

RED_2 at cathode: $3I_2 + 2e^- \text{----}\rightarrow 2I_3^-$ (6)

Here is Fig.3

Usually, the first pair of redox peaks attracts our more attention: the absolute value of cathodic reduction peak current density ($|I_{RED1}|$) is associated with the catalytic activity velocity and peak-to-peak separation (E_{PP}) reflects the catalytic activity of the redox reaction[3]. From Fig. 3(a), the PEDOT/Fe_3O_4-2 CE has the largest cathodic peak current (0.999mA·cm^{-2}), compared with PEDOT CE (0.906 mA·cm^{-2}), Pt CE (0.802mA·cm^{-2}), PEDOT/ Fe_3O_4-1 (0.936 mA·cm^{-2}) and PEDOT/ Fe_3O_4-3(0.804 mA·cm^{-2}). This means a faster redox reaction rate for I_3^- reduction on the PEDOT/Fe_3O_4-2 CE. Meanwhile, the Epp values decrease in the order of PEDOT/Fe_3O_4-2 (0.361V) < PEDOT/Fe_3O_4-3 (0.396V) < PEDOT/Fe_3O_4-1 (0.415V) < PEDOT (0.433V) <Pt (0.558V) <Fe_3O_4 (0.719V). As mentioned above, the CE based PEDOT/Fe_3O_4-2 is optimal and hybrid CEs has the larger $|I_{RED1}|$ and smaller Epp than the CE based pure material, illustrating that the moderate addition of Fe_3O_4 can improve catalytic activity velocity and catalytic activity of the redox reaction.

Fig. 3 (b) and Fig. 3 (c) investigated the relationships between the peak current density and the square root of the scan rate for PEDOT/Fe_3O_4-2 CE. According the two cyclic voltammeter, with increasing of scan rate, the cathodic peaks and anodic peaks current densities of PEDOT/Fe_3O_4-2 CEs gradually and regularly shifted to the negative and positive directions, respectively. Meanwhile, the current density versus the $(\text{scan rate})^{1/2}$ plots is almost linear, revealing that the redox reaction on PEDOT/Fe_3O_4-2 CEs is a diffusion limitation reaction, and no specific interaction between I^-/I_3^- redox couple and PEDOT/Fe_3O_4-2 CE. [33]

Electrochemical impedance spectroscopy (EIS) measurements were also exploited to analyze the symmetrical cell. A 50 μm Surlyn film was used to separate the films and to seal the cells and an acetonitrile electrolyte containing 0.05 M I_2, 0.1 M LiI, 0.6 M tetrabutyl ammonium iodide and 0.5 M TBP was injected into cells and a 50 μm Surlyn film was used to separate the two films and to seal the cells. The Nyquist curves of cells with PEDOT, PEDOT/Fe_3O_4, Fe_3O_4 are presented in Fig.3 (d) and the detailed EIS fitting parameters, obtained from the equivalent circuit in Fig.3 (e), are displayed in Table 3.

Here is Table 3

Typically，there two semicircles in the frequency range of 0.1-100KHz. The high frequency intercept of the left semicircle symbolizes the serial resistance (R_S) of symmetrical cells. One can see from table.3, the variation of Rs is negligible (10.7-12.7Ω) for all cells due to the same FTO substrate in cells. The charge transfer resistance (R_{CT}) at the CE/electrolyte interface and the electrical double-layer capacitor (CPE) are also represented in the left semicircle. In this study, the R_{CT} value for the PEDOT/Fe_3O_4 decreased with adding Fe_3O_4 just 2mg/ml in the precursor solution, but increased remarkably beyond that concentration. However, the change of the CPE has a reverse trend and is more strongly influenced by the Fe_3O_4 content. The Nernst diffusion impedance ($Z_{N)}$ of the triiodide/iodide couple in the electrolyte can be observed from the right semicircle in the low-frequency range arises from and it has a similar variation tendency with R_{CT}. Compared with Pt CE, the R_{CT} and Z_N of PEDOT/Fe_3O_4-2 are 2.22Ω·cm^2 and 0.822Ω·cm^2, respectively and these value are comparable to the value of Pt (R_{CT} =1.15Ω·cm^2 and Z_N =1.13Ω·cm^2). Furthermore, the values of 1/2CPE for PEDOT/Fe_3O_4-2 and Pt are 53.0μF·cm^2 and 1.20μF·cm^2, respectively.

Here is Fig.4

Tafel polarization measurements ,which is another mean to aid investigation the interfacial charge-transfer properties of the redox couple in the electrolyte on the CEs, were carried out by using two identical electrodes in an acetonitrile electrolyte containing 0.05 M I_2, 0.1 M LiI, 0.6 M tetrabutyl ammonium iodide and 0.5 M TBP. Fig.4 shows the Tafel polarization curves of PEDOT, PEDOT/Fe_3O_4-2, PEDOT/Fe_3O_4-1, PEDOT/Fe_3O_4-3, Pt, and Fe_3O_4 CEs.

A typical Tafel curve covers there zones: diffusion zone、tafel zone and potential zone. J_0 and J_{lim} can be obtained as the intercept of the extrapolated linear region of the curve when the over-potential is zero and in the curve at high potential (horizontal Part), respectively[34]. From the Fig.4，The slopes of the cathodic and anodic branches of the plots in the Tafel zone for the Pt CE are highest followed by PEDOT/Fe_3O_4-2. In the corresponding slopes, the slopes of Tafel curve for composite had no evident changes. According to Fig.4, the J_0 decreased in the order of PEDOT/Fe_3O_4-2 >Pt > PEDOT/Fe_3O_4-1> PEDOT > PEDOT/Fe_3O_4-3>Fe_3O_4. So the PEDOT/Fe3O4-2 electrode gives an excellent J_{lim} and Fe_3O_4 shows the lowest value of J_{lim}. PEDOT/Fe3O4-1, Pt, PDOT and PEDOT/Fe3O4-3 have medium values.

Here is Fig.5

4 Discussion:

SEM images, Fig.1, shows that small Fe_3O_4 content result in large lumps and some micropore-mesopore structure. The lumps size decreased as the Fe_3O_4 content increased. This is probably because the small amount Fe_3O_4 can be totally covered with PEDOT and bonded to lumps. The space between these large lumps can form into the micropore-mesopore structure. Meanwhile, plenty PEDOT can prevent Fe_3O_4 particles from connecting to one another and the electronic transmission channel is more consecutive. However, when the Fe_3O_4 content increase, there is not enough PEDOT to bond them or cover them completely. As a result, some areas for Fe_3O_4 to Fe_3O_4 connect or some areas are exposed, as proposed in Fig.5. More active area and more consecutive electronic transmission channel are answerable to the large Jsc and PCE of DSSC with PEDOT/Fe_3O_4-2. This is consist with the result of electrochemical testing. According to CV, the CE based PEDOT/Fe_3O_4-2 is optimal with a largest $|I_{RED1}|$ and smallest Epp, which suggests a best catalytic activity velocity and catalytic activity of the redox reaction.[23]

For the reduction of triiodide, R_{CT} is related to the catalytic activity of different CEs. The smaller the value of R_{CT} is, the better the catalytic activity of CE is. And CPE depends on the surface area of CE: a larger value of CPE means larger surface area of CE. When the concentration of Fe_3O_4 in the precursor solution was 2mg/ml, the CE had the smallest R_{CT} and the largest CPE. So, PEDOT/Fe_3O_4-2 also has the best performance and the parameter of PEDOT/Fe_3O_4-2 can be comparable to the parameter of Pt. What's more, FF is sensitive to the internal resistance in a DSSC, including both the Rs and the R_{CT}. The smaller the resistances is, the larger the value of FF is. According to the EIS, the FF of the DSSCs based PEDOT/Fe_3O_4-2 and the DSSCs based Pt are larger than that of other CEs, which mainly depends on the lower value of R_{CT}.

In Tafel curve, there are two important parameters related to the catalytic activity of the catalysts: the exchange current densities (J_0) and the limit diffusion current density (J_{lim})[35].

$$J_0 = \frac{RT}{nFR_{CT}} \quad (7)$$

$$D = \frac{J_{lim}L}{2nFC} \quad (8)$$

In the tafel zone, larger slopes of the cathodic and anodic branches of the plots means that the electrode can trigger the reduction of I_3^- to I^- more effectively. J_0 is relate to electrocatalytic activity. R_{CT} can be estimated as Eq (7) and the result trend is in good accordance with the lower charge-transfer resistance R_{CT} measured by EIS. J_{lim} is determined by the diffusion of the I^-/I_3^- redox couple in the electrolyte. Based on Eq (8), large J_{lim} reveals the large diffusion coefficient in the diffusion zone. Thus, the highest diffusion coefficient (D) value is achieved by PEDOT/Fe_3O_4-2 electrode, and this proves that PEDOT/Fe_3O_4-2 electrode holds a fast diffusion velocity of the redox couple in the electrolyte and the investigation from the Tafel polarization and EIS data are well consistent.

5 Conclusion:

The Situ polymerized PEDOT/Fe_3O_4 Composite was explored as a Pt free CE for DSSCs. This hybrid material showed excellent performance and highest power conversion efficiency (8.69%) was revealed by the DSSC with PEDOT/Fe3O4-2. In the same condition, the PCE of Pt DSSC is 8.35%. As shown by CV, EIS and Tafel respectively, the improvement of PCE should be due to the enhancement of the active area and the lower charge-transfer resistance of the film.

Reference:

1. Brian O'Regan , M. G. *Nature Photonics* **1991**, 737-740.

2. Liu, B.; Li, H. Y.; Die, L.; Zhang, X. H.; Fan, Z.; Chen, J. H. *Journal of Power Sources* **2009,** 186, (1), 62-66.
3. Lee, B.; Buchholz, D. B.; Chang, R. P. H. *Energy & Environmental Science* **2012,** 5, (5), 6941.
4. Wang, H.; Hu, Y. H. *Energy & Environmental Science* **2012,** 5, (8), 8182.
5. Li, Z.; Ye, B.; Hu, X.; Ma, X.; Zhang, X.; Deng, Y. *Electrochemistry Communications* **2009,** 11, (9), 1768-1771.
6. Sun, H. C.; Luo, Y. H.; Zhang, Y. D.; Li, D. M.; Yu, Z. X.; Li, K. X.; Meng, Q. B. *J Phys Chem C* **2010,** 114, (26), 11673-11679.
7. Wu, J.; Li, Q.; Fan, L.; Lan, Z.; Li, P.; Lin, J.; Hao, S. *Journal of Power Sources* **2008,** 181, (1), 172-176.
8. Zhu, C.; Min, H.; Xu, F.; Chen, J.; Dong, H.; Tong, L.; Zhu, Y.; Sun, L. *RSC Adv.* **2015,** 5, (104), 85822-85830.
9. Gong, F.; Wang, H.; Xu, X.; Zhou, G.; Wang, Z. S. *Journal of the American Chemical Society* **2012,** 134, (26), 10953-8.
10. Ma, X.; Yue, G.; Wu, J.; Lan, Z.; Lin, J.-Y. *RSC Adv.* **2015,** 5, (54), 43639-43647.
11. Chen, X.; Tang, Q.; He, B.; Lin, L.; Yu, L. *Angewandte Chemie* **2014,** 53, (40), 799-803.
12. He, B.; Meng, X.; Tang, Q. *ACS applied materials & interfaces* **2014,** 6, (7), 4812.
13. Thomas, S.; Deepak, T. G.; Anjusree, G. S.; Arun, T. A.; Nair, S. V.; Nair, A. S. *Journal of Materials Chemistry A* **2014,** 2, (13), 4474.
14. Arjunan, T. V.; Senthil, T. S. *Materials Technology: Advanced Performance Materials* **2013,** 28, (1/2), 9-14.
15. C. Kvarnström, H. N., S. Blomquist, H.J. Ahonen, J. Kankare, A. Ivaska, N.S. Sariciftci. *Synthetic Metals* **1999,** 101, (1-3), 66.
16. Damlin, P.; Kvarnström, C.; Ivaska, A. *Journal of Electroanalytical Chemistry* **2004,** 570, (1), 113-122.
17. Yohannes T, I. O. *Solar Energy Materials and Solar Cells* **1998,** 57, 193.
18. Hong, W.; Xu, Y.; Lu, G.; Li, C.; Shi, G. *Electrochemistry Communications* **2008,** 10, (10), 1555-1558.
19. Sekkarapatti Ramasamy, M.; Nikolakapoulou, A.; Raptis, D.; Dracopoulos, V.; Paterakis, G.; Lianos, P. *Electrochimica Acta* **2015,** 173, 276-281.
20. Xiao, Y.; Lin, J.-Y.; Tai, S.-Y.; Chou, S.-W.; Yue, G.; Wu, J. *Journal of Materials Chemistry* **2012,** 22, (37), 19919.
21. Koussi-Daoud, S.; Schaming, D.; Martin, P.; Lacroix, J.-C. *Electrochimica Acta* **2014,** 125, 601-605.
22. Xiao, Y.; Wu, J.; Yue, G.; Lin, J.; Huang, M.; Lan, Z.; Fan, L. *Electrochimica Acta* **2012,** 85, 432-437.
23. Maiaugree, W.; Pimanpang, S.; Towannang, M.; Saekow, S.; Jarernboon, W.; Amornkitbamrung, V. *Journal of Non-Crystalline Solids* **2012,** 358, (17), 2489-2495.
24. Wang, H.; Wei, W.; Hu, Y. H. *Journal of Materials Chemistry A* **2013,** 1, (22), 6622.
25. Yeh, M.-H.; Lin, L.-Y.; Li, Y.-Y.; Chang, J.; Chen, P.-W.; Lee, C.-P.; Ho, K.-C. *Japanese Journal of Applied Physics* **2012,** 51, 10NE01.
26. Wei, W.; Wang, H.; Hu, Y. H. *Journal of Materials Chemistry A* **2013,** 1, (45), 14350.
27. Wang, L.; Shi, Y.; Zhang, H.; Bai, X.; Wang, Y.; Ma, T. *Journal of Materials Chemistry A* **2014,** 2, (37), 15279.
28. Kiran Kisan Kokate, S. E. B., Sachin.A. Kulkarni. *INTERnational Journal of Innovative Technology and Research* **2015,** 3, (2).
29. Que, L.; Lan, Z.; Wu, W.; Wu, J.; Lin, J.; Huang, M. *Journal of Power Sources* **2014,** 268, 670-676.
30. Zheng, M.; Huo, J.; Tu, Y.; Wu, J.; Hu, L.; Dai, S. *Electrochimica Acta* **2015,** 173, 252-259.
31. Wu, J.; Tang, Z.; Huang, Y.; Huang, M.; Yu, H.; Lin, J. *Journal of Power Sources* **2014,** 257, 84-89.
32. Bi, E.; Chen, H.; Yang, X.; Peng, W.; Grätzel, M.; Han, L. *Energy & Environmental Science* **2014,** 7, (8), 2637.
33. Tang, Z**;** Wu, J.; Zheng, M.; Tang,Q; Liu,Q; Lin,J ; Wang,J. *RSC Adv.***2012,** 2, 4062–4064.
34. Yang, X. H.; Guo, J. W.; Yang, S.; Hou, Y.; Zhang, B.; Yang, H. G. *Journal of Materials Chemistry A* **2014,** 2, (3), 614.
35. Gong, F.; Xu, X.; Li, Z.; Zhou, G.; Wang, Z. S. *Chemical communications* **2013,** 49, (14), 1437-1446.

Figure and Table Captions

Fig.1. SEM of PEDOT (a) SEM of PEDOT/Fe_3O_4-1(b) SEM of PEDOT/Fe_3O_4-2 (c) SEM of PEDOT/Fe_3O_4-3 (d) (The bar is 100nm in the photographs) (e)section view SEM image of PEDOT/Fe_3O_4-2 (f) FTIR of EDOT and PEDOT (g) XRD of Fe_3O_4.

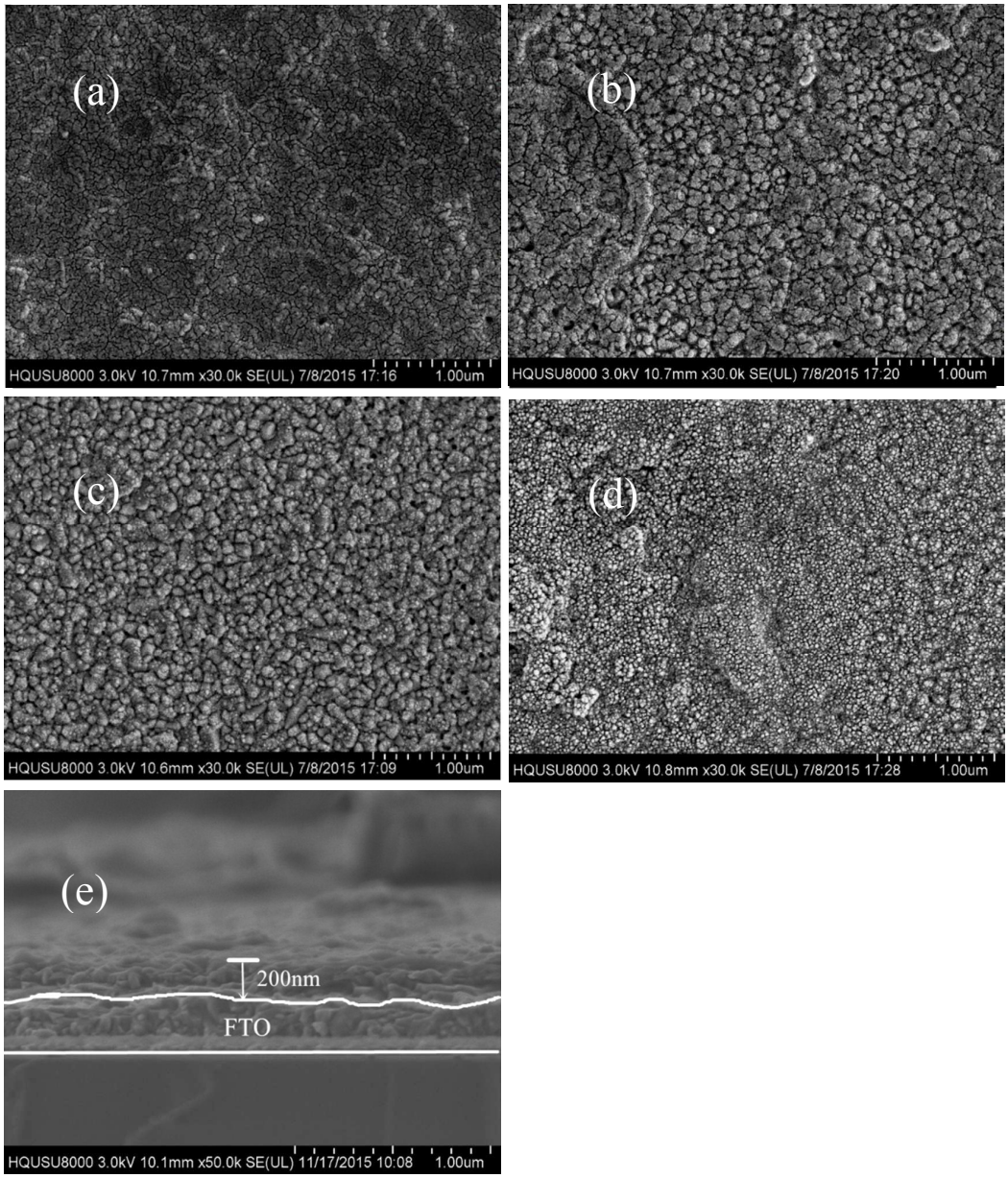

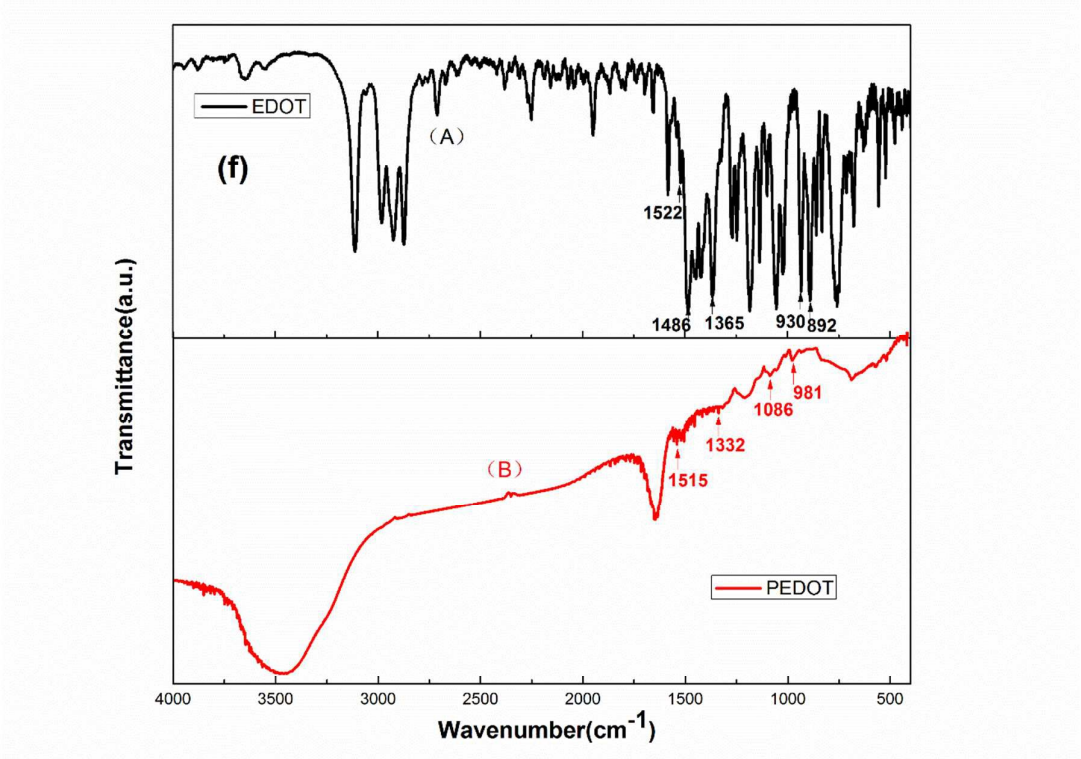

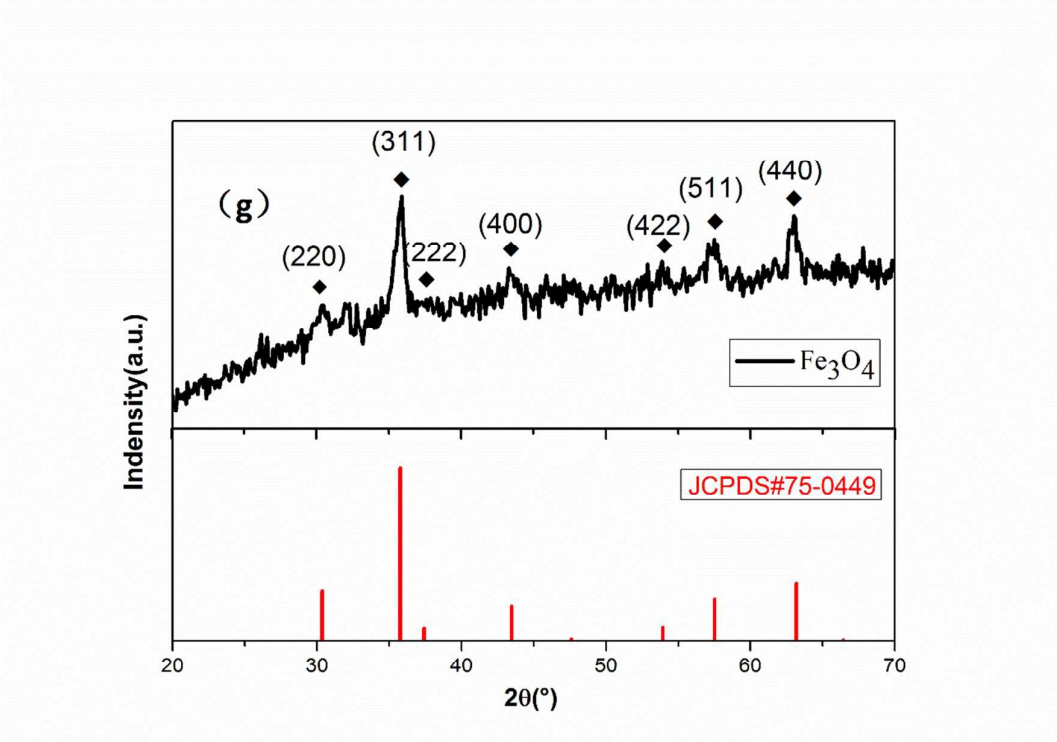

Fig.2 （a）Photocurrent-voltage curves of the DSSCs with different thinkness counter electrodes.
（b）Photocurrent-voltage curves of the DSSCs based on different counter electrodes.

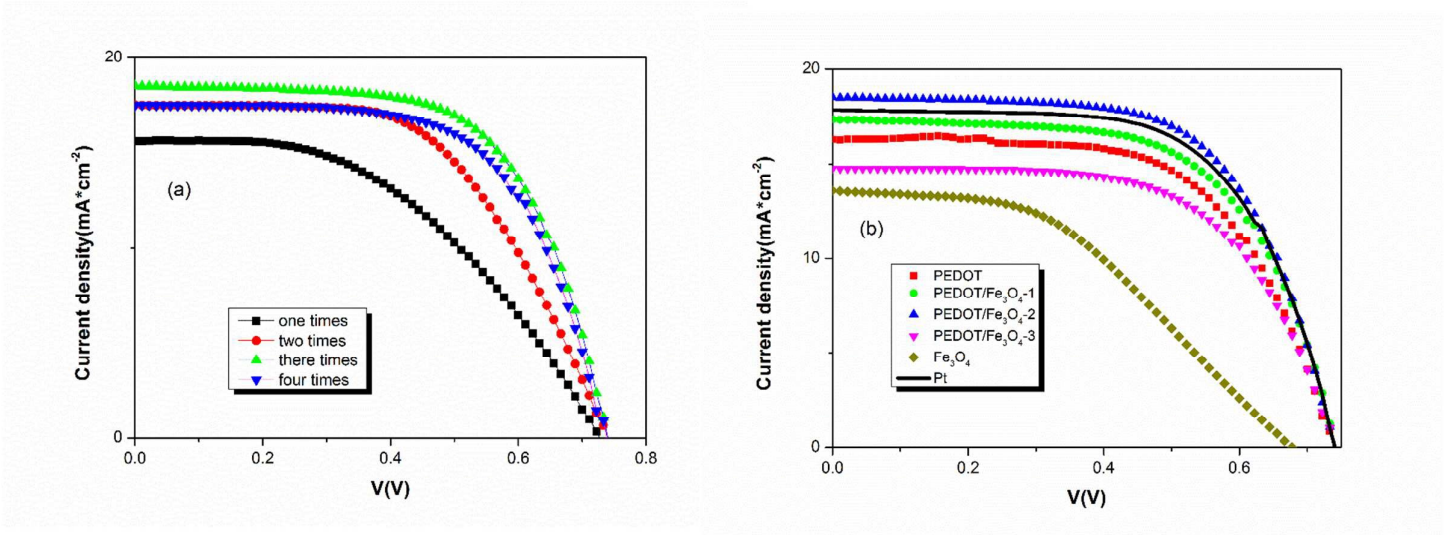

Fig.3 (a) CVs for the Pt, Fe_3O_4, PEDOT, PEDOT / Fe_3O_4-1, PEDOT/Fe_3O_4-2， PEDOT / Fe_3O_4-3 at the scan rate of 50 $mV{\cdot}s^{-1}$, (b) CVs for the PEDOT/Fe_3O_4-2 with different scan rates (from inner to outer: 0.025, 0.050, 0.075, 0.100, and 0.125 $V{\cdot}s^{-1}$), (c) The redox peak current versus square root of scan rate.(d) EIS measurements of the dummy cell fabricated with two identical PEDOT, PEDOT / Fe_3O_4-1, PEDOT/Fe_3O_4-2,PEDOT/Fe_3O_4-3, Pt, Fe_3O_4 and equivalent circuit model for I^-/I_3^- reaction (the scatter plots is obtained from experimental measurement and the line is the simulate the resultant spectra and the inset is the complete EIS of the dummy cell fabricated with two identical Fe_3O_4) (e) equivalent circuit model for I^-/I^{3-} reaction.

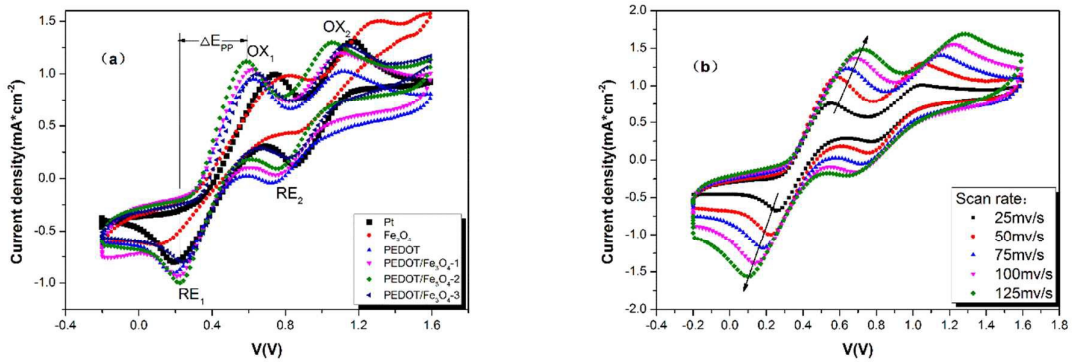

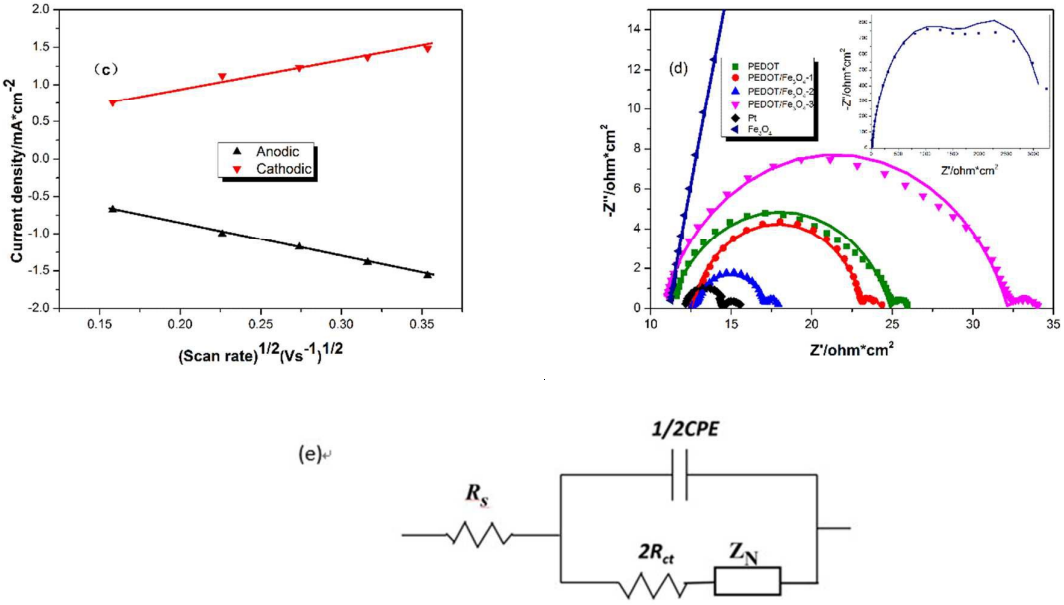

Fig.4. Tafel curves of the symmetrical dummy cells fabricated with two identical electrodes

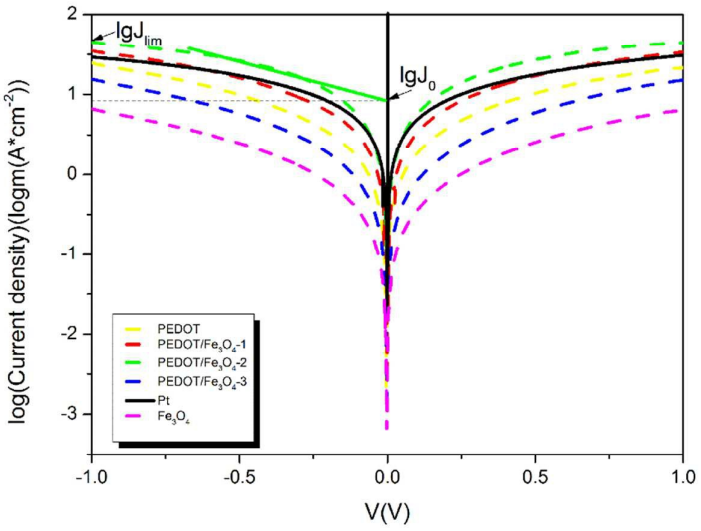

Fig.5 Schematic proposing PEDOT/Fe_3O_4 particle surfaces.

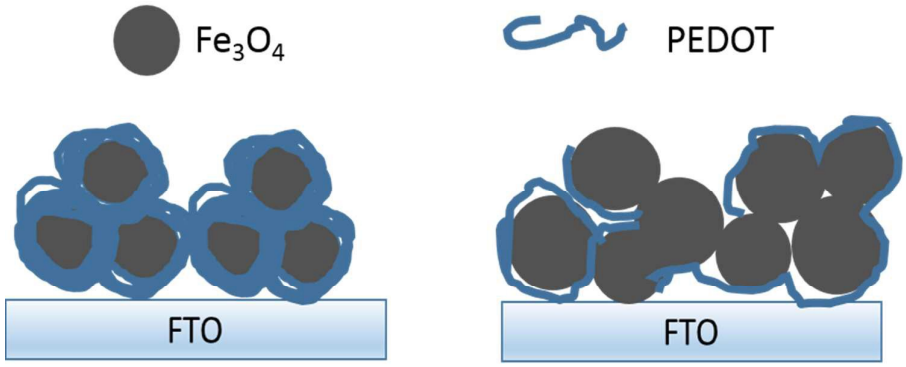

Table1 Photovoltaic parameters of the DSSCs with different thinkness counter electrodes.

Spin-casting times	V_{OC} (V)	J_{SC} ($mA.cm^{-2}$)	FF	PCE (%)
One	0.727	15.6	0.470	5.33
Two	0.742	17.5	0.562	7.31
Three	0.740	18.6	0.630	8.69
Four	0.738	17.6	0.630	8.16

Table2 Photovoltaic parameters of the DSSCs with different counter electrodes.

Electrodes	V_{OC} (V)	J_{SC} ($mA.cm^{-2}$)	FF	PCE (%)
PEDOT	0.740	16.3	0.615	7.40
PEDOT/Fe3O4-1	0.744	17.7	0.611	8.04
PEDOT/Fe3O4-2	0.740	18.6	0.630	8.69
PEDOT/Fe_3O_4-3	0.743	14.9	0.606	6.73
Fe_3O_4	0.677	13.8	0.430	4.02
Pt	0.742	17.9	0.631	8.38

Table 3 Electrochemical parameters for various counter electrodes

Electrodes	Test area (cm^2)	R_S ($\Omega \cdot cm^2$)	R_{CT} ($\Omega \cdot cm^2$)	1/2Cdl ($\mu F \cdot cm^2$)	Z_N ($\Omega \cdot cm^2$)
PEDOT	0.342	11.2	6.96	3.75	1.60
PEDOT/Fe_3O_4-1	0.350	12.6	5.27	11.8	0.960
PEDOT/Fe_3O_4-2	0.349	12.7	2.22	53.0	0.822
PEDOT/Fe_3O_4-3	0.359	10.7	10.8	3.64	1.63
Fe_3O_4	0.432	11.1	799	1.84	1668
Pt	0.349	12.14	1.16	1.20	1.13